SIAM J. Appl. Math.
Vol. 67, No. 6, pp. 1633–1653

CAVITATION ON DEFORMABLE GLACIER BEDS*

CHRISTIAN SCHOOF†

Abstract. The formation of water-filled cavities at the interface between a glacier and its bed can significantly affect the drainage of meltwater along the base of a glacier, which in turn is one of the most important controls on glacier sliding. In this paper, we analyze a mathematical model for cavity formation on deformable glacier beds. By contrast with the case of rigid glacier beds, the cavities described here are the result of an interfacial instability in coupled ice-sediment flow. This instability causes bumps on the ice-sediment interface to grow until normal stress in the lee of bed bumps drops to the local porewater pressure, at which point the ice begins to lose contact with the surface of the sediment. We extend the basic instability model to cover the case of cavity formation, and analyze the corresponding traveling wave problem. This takes the form of a viscous contact problem in which the obstacle on the boundary—the traveling bed bump caused by the initial instability—must be determined as part of the solution. A classical complex variable method allows the traveling wave problem to be cast as an eigenvalue problem which is straightforward to solve numerically. Our results show that solutions for different wavelengths can be obtained from an apparently unique solution to a scaled problem, and that the amplitude of traveling waves increases with wavelength, while their speed decreases with wavelength.

Key words. cavitation, contact problem, unilateral constraint, ice sheet

AMS subject classifications. 35J85, 76D07

DOI. 10.1137/050646470

1. Introduction.

The ice contained in many glaciers, especially those in mid-latitude mountain ranges, is close to the melting point, and meltwater generated at the glacier surface can reach the glacier bed through a network of conduits or *moulins* in the ice. The subsequent routing of meltwater via the glacier bed not only affects water discharge from the glacier, but also the dynamics of the glacier itself. The downslope motion of a glacier—which can be treated as a slowly flowing viscous body—consists of shearing in the ice and sliding at its base. High water pressure at the base of a glacier weakens the contact between ice and bed, and consequently reduces the amount of friction generated at the bed by sliding [7, 20, 17].

The presence of water-filled cavities at the interface between a glacier and its bed can play an important role in the drainage of meltwater along the glacier bed. The purpose of this paper is to analyze a model for the formation of such cavities. Previously developed mathematical models for subglacial cavitation [6, 17] deal with the flow of ice over a rigid glacier bed, and are essentially viscous analogues of elastic Signorini-type contact problems [13], although the subtle differences between the elastic and viscous cases appear to preclude a variational formulation for the latter. In contrast, the model considered here describes the spontaneous formation of cavities on a bed composed of deformable sediment. Consequently, the bed no longer represents a fixed "obstacle," but evolves as a result of stresses at the ice-sediment interface.

The instability mechanism which causes the formation of cavities in our model was

*Received by the editors November 30, 2005; accepted for publication (in revised form) May 30, 2007; published electronically September 14, 2007. This work was supported by the UK Engineering and Physical Sciences Research Council through a doctoral studentship at the Mathematical Institute, Oxford University, and by the U.S. National Science Foundation under grant DMS-03227943.
http://www.siam.org/journals/siap/67-6/64647.html
†Department of Earth and Ocean Sciences, University of British Columbia, 6339 Stores Rd., Vancouver, BC, V6T 1Z4 Canada (cschoof@eos.ubc.ca).

first proposed by Hindmarsh [11] and Fowler [8], and is described in detail in Schoof [19]. It relies on the pressure-dependence of the viscosity of subglacial sediment. (More precisely, sediment viscosity is assumed to depend on *effective pressure*, the difference between total pressure and porewater pressure, which controls how hard sediment grains are pressed together.) The mechanism may be summed up as follows: A shallow bump in the interface between ice and sediment causes a perturbation in the flow of ice over the bed, which leads to higher compressive normal stress being exerted on the upstream side of the bump than its lee. In turn, this causes increased effective pressure in the sediment layer upstream of the bump compared with downstream. Moreover, if the viscosity of the sediment is much lower than that of ice, the horizontal velocity of the interface is approximately constant (i.e., independent of position). Then, if the sediment rheology is such that flux in a thin sediment layer increases with effective pressure when the surface velocity of the layer is fixed, this implies that more sediment flows into the bump than out, causing it to grow.

This mechanism can be shown to work for a variety of viscous sediment rheologies, and numerical solutions of a simplified model show that growth of the instability is generally unbounded before the onset of cavitation [16, 19], which occurs when compressive normal stress in the lee of a bed bump drops to the local porewater pressure. In this paper, we will be concerned with the extension of that model to the case of cavitation. Our interest in this problem is largely motivated by the fact that cavity formation introduces a nonlinearity into the model, which may be sufficient to lead to bounded growth of the instability. Due to the complexity of the problem, we do not, however, consider the full time-dependent problem of cavity evolution, but restrict ourselves mostly to the case of traveling wave solutions, in the hope that these represent the fully evolved ice-bed interface.

The paper is structured as follows. In section 2, we describe the extension of the basic instability model to the case of cavitation. Subsequently, we formulate the traveling wave problem in section 3 and present a method of solution based on a classical complex variable approach. Results are discussed in section 4.

2. The model. We consider a simplified two-dimensional model for the spatially periodic flow of ice over a thin layer of water-saturated subglacial sediment in the absence of cavitation, as detailed in Schoof [19]. We set out the full time-dependent model here, first in the absence of cavitation and subsequently with cavitation. The analysis in this paper will, however, deal almost exclusively with the corresponding traveling wave problem, which we describe in the next section.

The basic assumptions of the model derived in [19] are the following. Ice is treated as an incompressible Newtonian fluid, while subglacial sediment is modeled as an incompressible shear-thinning viscous material whose viscosity additionally depends on *effective pressure*, defined as the difference between the ordinary pressure variable (the spherical part of the stress tensor in the language of continuum mechanics) and a prescribed porewater pressure. In particular, the rheology of subglacial sediment may be taken to be of the form

$$D_{ij} = KN^{-n}\tau^{m-1}\tau_{ij}, \tag{2.1}$$

where D_{ij} is strain rate, N is effective pressure, and τ_{ij} is deviatoric stress with second invariant $\tau = \sqrt{\tau_{ij}\tau_{ij}/2}$, while K, m, and n are positive constants. This rheological model has the qualitative features that strain rate increases with stress, as required for a viscous material, while strain rate decreases with effective pressure, corresponding to sediment grains less able to move past each other when pressed

harder together. The model described below makes a further approximation, treating only the parametric limit $n \approx m \gg 1$ in the rheology (2.1). This corresponds to a "nearly plastic" behavior, in which shear stress is only weakly dependent on strain rate [12]. As described in [19, section 7], this greatly simplifies expressions for volume flux in the sediment layer and shear stress at its surface, and leads to a more tractable ice flow problem.

Moreover, the model assumes that unstable waves generated at the ice-sediment interface have wavelengths that are long compared with the thickness of the sediment. Consequently, the sediment layer is treated as thin, with small surface slopes that allow the ice flow domain to be approximated by a half-space. Treating the sediment layer as thin further allows it to be described by a depth-integrated model that appears in the Stokes flow problem for the ice in the form of boundary conditions at the lower boundary. These boundary conditions can be derived essentially by integrating (2.1). For reasons of space, we refer to [19] for a more detailed derivation of the model.

Below, x and y are Cartesian coordinates parallel and perpendicular, respectively, to the mean bed elevation, while t is time and subscripts $_x$, $_y$, and $_t$ denote the corresponding partial derivatives. $\mathbf{u}(x, y, t)$ is a dimensionless velocity perturbation in the ice relative to a mean shearing flow, and $p(x, y, t)$ a dimensionless pressure perturbation about a mean hydrostatic pressure field. If a is the spatial period of the bed, $\mathbf{u} = (u, v)$ and p satisfy Stokes' equations on a semi-infinite strip in the upper half-plane:

$$\nabla^2 \mathbf{u} - \nabla p = \mathbf{0}, \qquad \nabla \cdot \mathbf{u} = 0 \qquad \text{on } (x, y) \in (0, a) \times (0, \infty), \tag{2.2}$$

with periodic boundary conditions applied at $x = 0$ and $x = a$. The interface between ice and sediment remains, at leading order, at $y = 0$ if waves on the bed are shallow. We denote the amplitude of these waves by $h(x, t)$, and sediment flux in the direction of the x-axis by $q(x, t)$. Effective pressure (the difference between confining normal stress and a prescribed porewater pressure) at the sediment surface will be denoted by $N(x, t)$, and shear stress at the ice-sediment interface by $\tau_b(x, t)$. Lastly, the velocity of the ice-sediment interface will be denoted by U. As before, all of these quantities have been scaled as in [19] and are dimensionless. Boundary conditions for the Stokes flow problems (2.2) are then

$$\left.\begin{aligned} u_y + v_x &\to \gamma^{-1}, \\ p &\to 0 \end{aligned}\right\} \qquad \text{as } y \to \infty, \tag{2.3}$$

$$\left.\begin{aligned} \gamma\,(u_y + v_x) &= \tau_b, \\ 1 + p - 2v_y &= N, \\ v &= U h_x + h_t \end{aligned}\right\} \qquad \text{on } y = 0. \tag{2.4}$$

Above, $\gamma > 0$ is the ratio of mean dimensional effective pressure to far-field shear stress. Hence γ^{-1} is a dimensionless far-field shear stress in $(2.3)_1$, while $(2.3)_2$ ensures that the pressure perturbation p vanishes at large distances from the bed. The boundary conditions $(2.4)_{1,2}$ at the bed relate the appropriate stress components in the Stokes problem to interfacial shear stress and effective pressure, while $(2.4)_3$ relates normal velocity at the bed to the evolution of bed wave amplitude h. h itself satisfies the evolution equation

$$h_t + q_x = 0. \tag{2.5}$$

As described at the beginning of this section, interfacial shear stress τ_b and flux q in the boundary conditions (2.4) must be determined through a model for the thin-

film flow of subglacial sediment. With the rheological specifications based on (2.1) described above, we find the appealingly simple (and *linear*) relationships

$$\tau_b(x,t) = N(x,t), \qquad q(x,t) = N(x,t). \tag{2.6}$$

Meanwhile, interface velocity is determined by a large-scale ice flow problem [18, 19], and in scaled terms we can simply set

$$U = 1, \tag{2.7}$$

while the x-component of the velocity $\mathbf{u} = (u, v)$ is subject to $\int_0^a u(x,0)\,\mathrm{d}x = 0$ (this condition being necessary to ensure a unique solution for $\mathbf{u}$).

As described above, the "constitutive relations" (2.6) are appropriate for a sediment layer flowing in simple shear with rheology given by (2.1) in the parametric limit $m \sim n \gg 1$ [19, section 7]. The relations are thus not completely general, though rheological tests support them [12]. As described in [16, 19] more general sediment rheologies can be introduced into the model simply by changing the prescriptions for τ_b and N in (2.6). We persist with (2.6) in part because it is supported by empirical evidence [12], and also because it is the simplest physically motivated choice we can make, yielding a linear relationships between τ_b, q, and N. However, as we point out in section 4, other rheological models for sediment may also be of practical interest, but these introduce the additional complication of nonlinear constitutive relations in (2.6), which are beyond the scope of this paper.

It is straightforward to show that the trivial solution $h(x,t) \equiv 0$ to (2.2)–(2.6) is unstable: The model admits Fourier mode solutions of the form $h(x,t) = \mathrm{Re}(\exp(ikx + \sigma t))$, where $\sigma = 2|k|^3/(1+2ik|k|)$ has a positive real part, and growth of the instability is apparently unbounded. However, this is physical only while effective pressure N is positive everywhere, which ensures that normal stress at the top of the sediment layer exceeds the porewater pressure within. Once $N = 0$ somewhere, compressive normal stress at the top of the sediment layer at that location equals porewater pressure, and porewater starts to leak out of the sediment. The ice loses contact with the sediment, and a water-filled cavity forms, as also happens in glacier sliding over undeformable beds [6, 17].

When a cavity has formed, different boundary conditions apply to (2.2) on those parts of the bed where cavities are present from those in effect where ice is in contact with sediment. Let the cavitated part of the bed at time t be denoted by $C(t)$, and the contact areas by $C'(t)$; the closure of $C \cup C'$ is then the interval $[0, a]$. The boundary conditions (2.4) together with the constraint $N \geq 0$ (which ensures that normal stress in contact areas cannot drop below the porewater pressure) still hold on $y = 0$, $x \in C'$. On cavitated parts of the bed, we require that effective pressure and shear stress vanish, as water pressure equals normal stress in the ice, and the water is assumed to be inviscid. This is tantamount to setting $\tau_b = N = 0$ in (2.4). In addition, the cavity roof must be above the surface of the sediment over cavitated parts of the bed and must satisfy a kinematic boundary condition analogous to $(2.4)_3$. We denote the dimensionless elevation of the cavity roof by $h_C(x,t)$ (see Figure 2.1) and assume that the cavity roof has a low aspect ratio, comparable with that of the sediment layer. Then we have [16, Chapter 6]

$$\left.\begin{aligned} 1 + p - 2v_y &= 0, \\ u_y + v_x &= 0, \\ v &= Uh_{Cx} + h_{Ct} \end{aligned}\right\} \qquad \text{on } y = 0,\ x \in C, \tag{2.8}$$

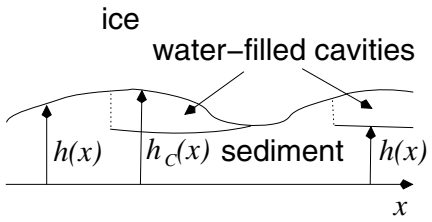

FIG. 2.1. *Illustration of cavity and contact areas, and the definition of h and h_C. The model assumes that bed slopes are small, so that the lower boundary of the ice flow domain can be reduced to $y = 0$ in dimensionless terms. Note that we generally assume discontinuities in h at downstream endpoints of contact areas. These sediment shocks are shown as dotted lines.*

while the absence of traction at the surface of the sediment in the cavities also implies

$$h_t = 0, \qquad q = 0, \qquad \text{on } y = 0,\ x \in C, \tag{2.9}$$

combined with the constraint $h_C > h$.

In addition to the boundary conditions (2.4) and (2.8) for the two-dimensional Stokes equations (2.2) and the evolution equation (2.5), we require jump conditions on h and h_C at the boundary points of C and C'. Based on physical considerations [16], we require that there be no discontinuities in the elevation of the lower boundary of the ice. Defining h_C everywhere as the scaled elevation of the base of the ice, so that $h_C(x) = h(x)$ for $x \in C'$, this implies that h_C is continuous across the endpoints of C and C'. It turns out that the same degree of continuity cannot be imposed on the sediment wave amplitude h, and a discontinuity must be expected at at least one endpoint of each individual contact area. Such discontinuities are not entirely unexpected: For the somewhat similar problem of dune formation in deserts and on river beds [9], the equivalent would be a slip face. The flow of sediment close to a contact point where h is discontinuous cannot be resolved by our thin-film approximation for the sediment. However, instead of attempting to solve an extremely complicated local sediment flow problem, we argue heuristically. We assume that the propagation speed of the contact point is determined by a Rankine–Hugeniot condition which ensures conservation of sediment:

$$V_s = [q]^+_-/[h]^+_-, \tag{2.10}$$

where V_s is the propagation speed of the sediment shock and $[\cdot]^+_-$ denotes the jump in the bracketed quantity across the shock. With $q = N$, it follows from the continuity of h_C and the inequality constraints on h and N that the jump in q must have the same sign as the jump in h, and hence the sediment shock must propagate downstream with $V_s > 0$.

If there were a sediment shock at the upstream end of a contact area, then effective pressure would be positive downstream of the contact point and zero in the cavity. The resulting pressure difference should drive a local sediment flow (not resolved by our thin-film approximation) into the cavity, that is, in the upstream direction and therefore opposite to that required by (2.10). As a consequence, we permit discontinuities in h only at the downstream ends of contact areas and require that h be continuous across the upstream end of each contact area.

As we shall see below, these jump conditions on h and h_C lead to an apparently

well-posed traveling wave problem. Whether or not they can in fact be applied to the general time-dependent problem is a matter for future research.

3. Traveling waves. In what follows, we consider solutions in which h and h_C depend on x and t only through the traveling wave coordinate

$$\eta = x - Vt, \tag{3.1}$$

where $V > 0$ is the unknown pattern speed of the traveling wave. Note that negative pattern speeds are not possible because sediment shocks must propagate downstream, as explained above. Writing $\hat{\nabla} = (\partial/\partial\eta, \partial/\partial y)$, the model can then be cast in the form

$$\hat{\nabla}^2\mathbf{u} - \hat{\nabla}p = \mathbf{0}, \qquad \hat{\nabla}\cdot\mathbf{u} = 0 \qquad \text{on } (\eta, y) \in (0, a) \times (0, \infty), \tag{3.2}$$

$$\left.\begin{aligned} u_y + v_\eta &\to \gamma^{-1}, \\ p &\to 0 \end{aligned}\right\} \qquad \text{as } y \to \infty, \tag{3.3}$$

$$\left.\begin{aligned} \gamma\,(u_y + v_\eta) &= \tau_b, \\ 1 + p - 2v_y &= N, \\ v &= (U - V)h', \\ q' - Vh' &= 0, \\ N &\geq 0 \end{aligned}\right\} \qquad \text{on } \eta \in \hat{C}',\ y = 0, \tag{3.4}$$

$$\left.\begin{aligned} u_y + v_\eta &= 0, \\ 1 + p - 2v_y &= 0, \\ v &= (U - V)h_C', \\ h' &= 0, \\ h_C &> h \end{aligned}\right\} \qquad \text{on } \eta \in \hat{C},\ y = 0, \tag{3.5}$$

$$q = N \qquad \text{on } \eta \in \hat{C}', \tag{3.6}$$

$$q = 0 \qquad \text{on } \eta \in \hat{C}, \tag{3.7}$$

$$\tau_b = N, \qquad U = 1. \tag{3.8}$$

Here primes on h, h_C, and q denote differentiation with respect to η, and $\hat{C}' = C'(0)$ and $\hat{C} = C(0)$ denote contact and cavity areas, respectively, at the bed in the (η, y) coordinate system. In addition, we consider only the case of a single cavity per bed period, and without further loss of generality we can set

$$\hat{C}' = (0, b), \qquad \hat{C} = (b, a), \tag{3.9}$$

where the contact point $\eta = b$ is to be determined as part of the solution. As before, we impose periodic boundary conditions on $\eta = 0$ and $\eta = a$. The continuity requirements on h and h_C at the contact points are

$$h(0^+) = h(a^-) = h_C(a^-), \qquad h(b^-) = h_C(b^+), \tag{3.10}$$

where superscripts $+$ and $-$ indicate limits taken from above and below, respectively (and where, in an abuse of notation, we have replaced the arguments (x, t) by η). Lastly, the jump condition (2.10) for a sediment shock at $\eta = b$ propagating at the pattern speed $V_s = V$ becomes

$$V = -q(b^-)/(h(b^+) - h(b^-)), \tag{3.11}$$

where we recognize that $q(b^+) = 0$ from (3.7).

Some small simplifications are immediately possible. As the model is invariant under changes of h and h_C by the same constant, we can without loss of generality set $h = 0$ in $\hat{C}$ by $(3.5)_4$. $(3.4)_4$ and (3.11) combined then require that

$$q = Vh \qquad \text{on } \hat{C}, \tag{3.12}$$

and the jump conditions on h and h_C become

$$h(0^+) = h_C(a^-) = 0, \qquad h(b^-) = h_C(b^+). \tag{3.13}$$

Equations (3.12) and (3.13) then replace $(3.4)_4$, (3.10), and (3.11) in the subsequent analysis.

The model described above is in many ways similar to the viscous contact problems considered by Fowler [6] and Schoof [17], in the sense that we have a Stokes flow problem with mixed boundary conditions prescribed on parts of the boundary which are not known a priori but must be found as part of the solution so as to satisfy the inequality constraints $(3.4)_5$ and $(3.5)_5$. This introduces an important nonlinearity into the problem which is missing in the original linear evolution problem and, as we shall see, allows for the existence of (nontrivial) traveling wave solutions, which are not possible without cavitation. The crucial difference between the model considered here and that in [6, 17] is that the bed elevation h is not fixed here but forms part of the solution. This renders the problem considerably more complicated.

The remainder of this section will be devoted to constructing a method of solution. Our approach consists of the following steps. First, we represent the solution of the Stokes equations (3.2) in terms of complex potentials. When mapped conformally so as to make use of the periodic boundary conditions at the sides of the domain, the boundary conditions (3.3)–(3.5) lead to a pair of Hilbert problems for these complex potentials, which admit explicit solutions in terms of the unknown functions N and τ_b and the contact point position b. Finally, applying the remaining conditions (3.8), (3.12), and (3.13) allows the problem of finding N and τ_b to be recast as an eigenvalue problem for h (which simultaneously determines the pattern speed V), and b can be determined through an additional integral constraint which ensures that the lower ice surface has no discontinuities.

3.1. Complex variable formulation. We introduce a stream function ψ such that

$$u = \psi_y + y/\gamma, \qquad v = -\psi_\eta, \tag{3.14}$$

where the additional shearing term in the definition of u accounts for the far-field shear stress. Further, we define the complex variables $z = \eta + iy$ and $\overline{z} = \eta - iy$. ψ satisfies the biharmonic equation, which can be written in terms of z and $\overline{z}$ as

$$\hat{\nabla}^4\psi = 4\psi_{zz\overline{z}\overline{z}} = 0. \tag{3.15}$$

Using standard methods in complex analysis [5], ψ can be shown to take the general form

$$\psi = (\overline{z} - z)\theta(z) + \phi(z) + (z - \overline{z})\overline{\theta(z)} + \overline{\phi(z)} \tag{3.16}$$

for z in the semi-infinite strip $0 < \eta < a$, $0 < y$, where θ and ϕ are analytic functions and an overbar denotes complex conjugation. Furthermore, the Stokes equations (3.2) become

$$\hat{\nabla}^2\psi_y = p_\eta, \qquad -\hat{\nabla}^2\psi_\eta = p_y, \tag{3.17}$$

which are the Cauchy–Riemann relations for $p + i\hat{\nabla}^2\psi$ (i.e., pressure p and vorticity $\hat{\nabla}^2\psi$ are harmonic conjugates). Using standard differentiation rules [5], $\hat{\nabla}^2\psi = 4(\theta'(z) + \overline{\theta'(z)}) = 8\mathrm{Im}(i\theta'(z))$, where a prime denotes differentiation. Consequently,

$$p = C_0 + 8\mathrm{Re}(i\theta'(z)) = C_0 + 4i(\theta'(z) - \overline{\theta'(z)}), \tag{3.18}$$

where C_0 is a real constant. The value of this constant can be chosen arbitrarily: If $C_0 \neq 0$, we can add $iC_0 z/8$ to $\theta(z)$ and simultaneously add $iC_0 z^2/8$ to $\phi(z)$ while leaving the stream function ψ in (3.16) unchanged. By redefining θ and ϕ in this way, we ensure that $C_0 = 0$ in (3.18), and we will henceforth assume this to be the case.

In order to satisfy the periodic boundary conditions imposed on the problem, it suffices to ensure that u, v, and p can be extended to sufficiently smooth functions in the half-space $y > 0$, which are periodic in η with period a. Anticipating therefore that p and vorticity $\nabla^2\psi$ can be extended to harmonic functions which are appropriately periodic, we conclude that $\theta'(z)$ can be continued to an analytic function in the upper half-plane which is periodic in $\mathrm{Re}(z)$ with period a. Furthermore, we have for $y > 0$

$$u = 4y\mathrm{Re}\left[\theta'(z)\right] + 2\mathrm{Im}\left[2\theta(z) - \phi'(z)\right], \tag{3.19}$$

$$v = -4y\mathrm{Im}\left[\theta'(z)\right] - 2\mathrm{Re}\left[\phi'(z)\right]. \tag{3.20}$$

Hence, if $\theta'(z)$ can be continued to a periodic analytic function, it suffices to ensure in addition that $\mathrm{Im}[2\theta(z) - \phi'(z)]$ and $\mathrm{Re}[\phi'(z)]$ can be extended to harmonic functions in the upper half-plane with period a in $\mathrm{Re}(z)$. From the periodicity of $\mathrm{Re}[\phi'(z)]$, it follows that $\phi''(z)$ can be continued to an appropriately periodic analytic function in the entire upper half-plane $\mathrm{Im}(z) > 0$. Moreover, the periodicity of $\mathrm{Re}[\phi'(z)]$ and $\mathrm{Im}[2\theta(z) - \phi'(z)]$ are equivalent to

$$\mathrm{Re}\left[\phi'(a+iy) - \phi'(iy)\right] = \mathrm{Re}\left[\int_0^a \phi''(\eta + iy)\,\mathrm{d}\eta\right] = 0, \tag{3.21}$$

$$\mathrm{Im}\left[\int_0^a 2\theta'(\eta + iy) - \phi''(\eta + iy)\,\mathrm{d}\eta\right] = 0 \tag{3.22}$$

for all $y > 0$.

We complete our complex variable formulation by casting the boundary conditions (3.3)–(3.5) in terms of θ and ϕ. At the lower boundary $y = 0$

$$2i(\phi''(\eta) - \overline{\phi''(\eta)}) = \begin{cases} N(\eta) - 1, & \eta \in \hat{C}', \\ -1, & \eta \in \hat{C}, \end{cases} \tag{3.23}$$

$$2(2\theta'(\eta) - \phi''(\eta) + 2\overline{\theta'(\eta)} - \overline{\phi''(\eta)}) = \begin{cases} \gamma^{-1}\left(\tau_b(\eta) - 1\right), & \eta \in \hat{C}', \\ -\gamma^{-1}, & \eta \in \hat{C}, \end{cases} \tag{3.24}$$

$$-(\phi'(\eta) + \overline{\phi'(\eta)}) = \begin{cases} (U - V)h'(\eta), & \eta \in \hat{C}', \\ (U - V)h'_C(\eta), & \eta \in \hat{C}, \end{cases} \tag{3.25}$$

combined with (3.8), (3.12), and (3.13). Naturally, θ', ϕ', and ϕ'' are defined on the real axis as boundary values taken as z approaches the axis from above. As $\mathrm{Im}(z) = y \to \infty$, we have from (3.3)

$$4i\left[\theta'(z) - \overline{\theta'(z)}\right] \to 0, \tag{3.26}$$

$$-2\left[\phi''(z) - 2iy\theta''(z) - 2\theta'(z) + \overline{\phi''(z)} + 2iy\overline{\theta''(z)} - 2\overline{\theta'(z)}\right] \to 0. \tag{3.27}$$

3.2. Reformulation as a Hilbert problem. In order to exploit the periodicity of the problem, and to obtain a straightforwardly solved pair of Hilbert problems for proxies of θ' and ϕ'', we map conformally to the ζ-plane as

$$\zeta = \exp(i2\pi z/a), \qquad \xi = \exp(i2\pi\eta/a), \tag{3.28}$$

where $0 < \eta = \mathrm{Re}(z) < a$. We denote by Γ and Γ' the images of $\hat{C}$ and $\hat{C}'$ under this mapping. Γ and Γ' are then disjoint arcs of the unit circle in the ζ-plane, and the closure of $\Gamma \cup \Gamma'$ is the unit circle itself. We also define $\tilde{N}(\xi) = N(\eta)$, $\tilde{\tau}_b(\xi) = \tau_b(\eta)$, and let

$$\Omega(\zeta) = \begin{cases} \overline{\phi''(\overline{z})}, & |\zeta| > 1, \\ \phi''(z), & 0 < |\zeta| < 1, \end{cases} \tag{3.29}$$

$$\omega(\zeta) = \phi'(z), \qquad 0 < |\zeta| < 1, \tag{3.30}$$

$$\Theta(\zeta) = \begin{cases} \overline{\theta'(\overline{z})}, & |\zeta| > 1, \\ \theta'(z), & 0 < |\zeta| < 1. \end{cases} \tag{3.31}$$

From the Schwarz reflection principle and the periodicity requirements above, it follows that Ω and Θ are analytic in the finite ζ-plane cut along the unit circle and punctured at the origin, while ω is analytic inside the open unit disk cut along the nonnegative part of the real axis in the ζ-plane, where ω may be discontinuous because we know only that $\mathrm{Re}(\phi')$ is periodic. As we shall show later, ω is in fact analytic across that branch cut. Moreover, using $\mathrm{d}/\,\mathrm{d}z = (i2\pi/a)\zeta\,\mathrm{d}/\,\mathrm{d}\zeta$,

$$\Omega(\zeta) = (i2\pi/a)\zeta\omega'(\zeta) \tag{3.32}$$

for $|\zeta| < 1$, except on the branch cut.

The boundary conditions (3.23)–(3.25) become

$$2i\left[\Omega^+(\xi) - \Omega^-(\xi)\right] = \begin{cases} \tilde{N}(\xi) - 1, & \xi \in \Gamma', \\ -1, & \xi \in \Gamma, \end{cases} \tag{3.33}$$

$$2\left[2\Theta^+(\xi) - \Omega^+(\xi) + 2\Theta^-(\xi) - \Omega^-(\xi)\right] = \begin{cases} \gamma^{-1}(\tilde{\tau}_b(\xi) - 1), & \xi \in \Gamma', \\ -\gamma^{-1}, & \xi \in \Gamma, \end{cases} \tag{3.34}$$

$$-2\mathrm{Re}(\omega^+(\xi)) = \begin{cases} (U - V)h'(\eta), & \xi \in \Gamma', \\ (U - V)h'_C(\eta), & \xi \in \Gamma, \end{cases} \tag{3.35}$$

where superscripts + and − denote limits taken as the unit circle is approached from within and without, respectively. The first two of these equations take the form of standard Hilbert problems, whose solutions depend on the behavior of Ω and Θ at infinity. Because of the symmetry inherent in the definitions of Ω and Θ, their behavior at infinity is determined by their behavior at the origin. From (3.27), we have for $\zeta \to 0$

$$4i\left[\Theta(\zeta) - \overline{\Theta(\zeta)}\right] \to 0, \tag{3.36}$$

$$\Omega(\zeta) + \overline{\Omega(\zeta)} - 2\Theta(\zeta) - 2\overline{\Theta(\zeta)} - 2\log|\zeta|\left[\zeta\Theta'(\zeta) + \overline{\zeta\Theta'(\zeta)}\right] \to 0. \tag{3.37}$$

It follows from (3.36) that Θ is analytic at the origin with $\Theta(0) = C_1$, where C_1 is a real constant. Hence $\lim_{\zeta\to 0} \zeta\log|\zeta|\Theta'(\zeta) = 0$, and from (3.37) it follows that Ω is also analytic at the origin with $\Omega(0) = 4C_1 + iC_2$, where C_2 is another real constant.

It can then be shown from the periodicity requirements (3.22) that both C_1 and C_2 vanish. Specifically, (3.22) can be written as

$$\mathrm{Re}\left[\frac{a}{i2\pi}\oint_L \frac{\Omega(\zeta)\,\mathrm{d}\zeta}{\zeta}\right] = \mathrm{Im}\left[\frac{a}{i2\pi}\oint_L \frac{[2\Theta(\zeta)-\Omega(\zeta)]}{\zeta}\,\mathrm{d}\zeta\right] = 0, \tag{3.38}$$

where L is a circular contour about the origin with radius less than 1, traversed anticlockwise. Applying the residue theorem, this implies that $C_1 = C_2 = 0$, and hence

$$\Omega(0) = \Theta(0) = 0. \tag{3.39}$$

From (3.39) and the definitions of Ω and Θ in (3.31) it finally follows that

$$\Omega(\zeta) = \overline{\Omega(1/\bar{\zeta})}, \qquad \Omega(\infty) = 0, \qquad \Theta(\zeta) = \overline{\Theta(1/\bar{\zeta})}, \qquad \Theta(\infty) = 0, \tag{3.40}$$

which taken together also ensure the appropriate behavior at the origin.

We can now solve (3.33), (3.34), and (3.40) explicitly in terms of the as yet unknown effective pressure $N(\eta)$ and shear stress $\tau_b(\eta)$. For the sake of simplicity, define Ξ as a proxy for Θ through

$$\Xi(\zeta) = \begin{cases} 2\Theta(\zeta) - \Omega(\zeta), & |\zeta| < 1, \\ -2\Theta(\zeta) + \Omega(\zeta), & |\zeta| > 1, \end{cases} \tag{3.41}$$

so that (3.34) becomes

$$\Xi^+(\xi) - \Xi^-(\xi) = \begin{cases} \gamma^{-1}(\tilde{\tau}_b(\xi) - 1), & \xi \in \Gamma', \\ -\gamma^{-1}, & \xi \in \Gamma, \end{cases} \tag{3.42}$$

subject to $\Xi(\infty) = 0$, $\Xi(\zeta) = -\overline{\Xi(1/\bar{\zeta})}$. Assuming that $\tilde{N}$ and $\tilde{\tau}_b$ are Hölder continuous and bounded on Γ' (we exclude the possibility of integrable singularities at the endpoints of Γ' because N and τ_b are related to h through (3.8) and (3.12), and h is clearly bounded), (3.33) and (3.42) admit solutions vanishing at infinity of the form (see [14])

$$\Omega(\zeta) = -\frac{1}{4\pi}\int_{\Gamma'} \frac{\tilde{N}(\xi)}{\xi - \zeta}\,\mathrm{d}\xi + \frac{1}{4\pi}\int_{\Gamma\cup\Gamma'} \frac{1}{\xi-\zeta}\,\mathrm{d}\xi, \tag{3.43}$$

$$\Xi(\zeta) = \gamma^{-1}\left[\frac{1}{2\pi i}\int_{\Gamma'} \frac{\tilde{\tau}_b(\xi)}{\xi-\zeta} - \frac{1}{2\pi i}\int_{\Gamma\cup\Gamma'} \frac{1}{\xi-\zeta}\,\mathrm{d}\xi\right], \tag{3.44}$$

where integrals over Γ and Γ' are taken (here and in what follows) as the unit circle is traversed in the anticlockwise direction. Note that the second integral on the right-hand side of each equation may be recognized as $\int_{\Gamma\cup\Gamma'}(\xi-\zeta)^{-1}\,\mathrm{d}\xi = 2\pi i$ if ζ is inside the unit circle, $\int_{\Gamma\cup\Gamma'}(\xi-\zeta)^{-1}\,\mathrm{d}\xi = 0$ for ζ outside the unit circle.

It remains to ensure that Ω and Ξ satisfy $(3.40)_{1,3}$. Using the fact that $\tilde{N}$ is real, while $\bar{\xi} = 1/\xi$ and $\overline{\mathrm{d}\xi} = -1/\xi^2\,\mathrm{d}\xi$, it follows after some manipulation that

$$\overline{\Omega(1/\bar{\zeta})} = -\frac{1}{4\pi}\int_{\Gamma'} \tilde{N}(\xi)\left[\frac{1}{\xi-\zeta} - \frac{1}{\xi}\right]\mathrm{d}\xi + \frac{1}{4\pi}\int_{\Gamma'\cup\Gamma}\left[\frac{1}{\xi-\zeta} - \frac{1}{\xi}\right]\mathrm{d}\xi, \tag{3.45}$$

with a similar expression for $\overline{\Xi(1/\bar{\zeta})}$. In order to satisfy $\Omega(\zeta) = \overline{\Omega(1/\bar{\zeta})}$ and $\Xi(\zeta) = -\overline{\Xi(1/\bar{\zeta})}$, we therefore require

$$\int_{\Gamma'} \frac{\tilde{N}(\xi)}{\xi}\,\mathrm{d}\xi - \int_{\Gamma\cup\Gamma'} \frac{\mathrm{d}\xi}{\xi} = 0, \qquad \int_{\Gamma'} \frac{\tilde{\tau}_b(\xi)}{\xi}\,\mathrm{d}\xi - \int_{\Gamma\cup\Gamma'} \frac{\mathrm{d}\xi}{\xi} = 0. \tag{3.46}$$

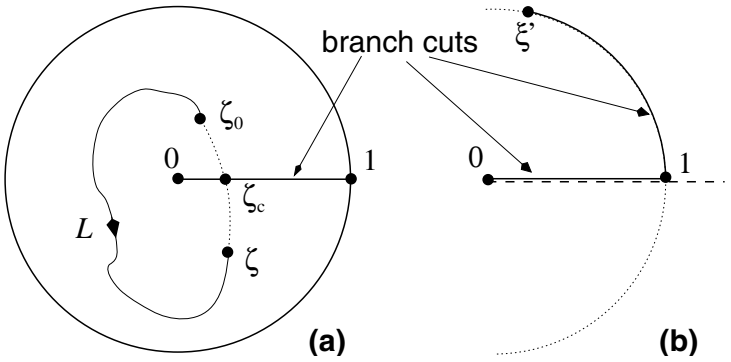

FIG. 3.1. *The contour L in* (3.48) *is shown in panel* (a)*, where solid lines indicate branch cuts in ω. The branch cuts for* $\log(\xi'/\zeta - 1)$ *(solid line) and* $\log(\zeta)$ *(dashed line) are shown in panel* (b).

In real terms, these equations are simply

$$\frac{1}{a}\int_0^b N(\eta)\,\mathrm{d}\eta = 1, \qquad \frac{1}{a}\int_0^b \tau_b(\eta)\,\mathrm{d}\eta = 1, \tag{3.47}$$

which physically state that the mean shear stress at the ice-sediment interface is the far-field shear stress, and that mean effective pressure is fixed by hydrostatic ice overburden and by porewater pressure in the bed (the difference between the two being scaled to unity). With the particular prescription of τ_b in (3.8), the two equations in (3.47) are identical, and we are left with the single constraint $(3.47)_1$, which states that mean effective pressure at the bed is fixed at unity.

The expressions for Ω and Ξ in (3.43) and (3.44) as well as the solvability constraints in (3.47) contain the unknown functions N and τ_b, which depend on sediment thickness h through the constitutive relations (3.6) and (3.8) as well as through (3.12), while h conversely depends on N and τ_b through (3.35). Moreover, the limits of integration appearing in (3.43) and (3.44) are not known a priori, as we have yet to determine the position of the contact point $\eta = b$. In the next section, we show how h (and hence N and τ_b) can be calculated from an eigenvalue problem arising from (3.35), which also determines the pattern speed V as its eigenvalue. Additionally, the continuity requirements in (3.13) allow us to derive an integral constraint which fixes the position of the contact point b.

3.3. Reduction to an eigenvalue problem. We exploit (3.35), (3.32), and (3.43) as well as (3.6), (3.12), (3.13) and the inequality constraints in (3.4) and (3.5) in order to obtain integral equations for h and h_C. Our first task is to calculate ω, which determines the bed slopes h' and h'_C through (3.35). For ζ_0 and ζ in the open unit disk of the ζ-plane cut along the nonnegative half of the real axis, where ω has a branch cut, we have from (3.32)

$$\omega(\zeta) - \omega(\zeta_0) = \frac{a}{i2\pi}\int_L \frac{\Omega(\zeta')}{\zeta'}\,\mathrm{d}\zeta', \tag{3.48}$$

where primes on ζ' indicate a dummy variable, not differentiation. L is any arc connecting ζ_0 to ζ such that L lies entirely in the open unit disk and does not cross the branch cut in ω (see Figure 3.1). It follows from (3.48) that ω is in fact continuous and therefore analytic across that branch cut: Let ζ_c lie on the branch cut, and let

ζ_0 and ζ approach ζ_c from the first and fourth quadrants, respectively. In the limit, L becomes a closed contour encircling the origin (Figure 3.1), and from the residue theorem we have

$$\omega(\zeta) - \omega(\zeta_0) \to a\Omega(0) = 0, \tag{3.49}$$

so $\omega(\zeta_c)$ can be assigned a unique limiting value regardless of which side the real axis is approached from. As a corollary, we can in fact allow the arc L above to cross the positive half of the real axis (which later allows us to establish that $\omega(\zeta)$ has a unique limit when $\zeta \to 1$ from inside the unit circle).

Using (3.43), we can evaluate the integral in (3.48) explicitly:

$$\begin{aligned}\omega(\zeta) - \omega(\zeta_0) = &-\frac{a}{i8\pi^2}\int_{\Gamma'} \tilde{N}(\xi')\left[\log\left(\frac{\xi'}{\zeta_0} - 1\right) - \log\left(\frac{\xi'}{\zeta} - 1\right)\right]\frac{\mathrm{d}\xi'}{\xi'} \\ &+ \frac{a}{4\pi}[\log(\zeta) - \log(\zeta_0)],\end{aligned} \tag{3.50}$$

where for definiteness $\log(\xi'/\zeta_0 - 1)$ and $\log(\xi'/\zeta - 1)$ denote a branch of the logarithm which has a branch cut as indicated in Figure 3.1. Similarly, $\log(\zeta_0)$ and $\log(\zeta)$ denote a branch which has a branch cut along the positive half of the real axis.

Next, we let $\zeta \to \xi$ and $\zeta_0 \to 1$ from inside the unit circle. It is easy to show from (3.48), Cauchy's theorem, and the continuity properties of Ω [14, pp. 53–55 and Chapter 4] that the limit $\omega^+(\xi)$ exists and is continuous as a function of ξ for all ξ on the unit circle. Importantly, this result holds true at both endpoints of Γ', where $\xi = 1$ and $\xi = \exp(i2\pi b/a)$ (with continuity at $\xi = 1$ resulting from the continuity of ω across the real axis). Using (3.35) and (3.50) and taking care with the branches of the logarithms involved, we find after some elementary manipulations that

$$\begin{aligned}-2\mathrm{Re}(\omega^+(\xi) - \omega^+(1)) &= -\frac{1}{2\pi}\int_0^b N(\eta')\log\left|\frac{\sin(\pi(\eta' - \eta)/a)}{\sin(\pi\eta'/a)}\right|\mathrm{d}\eta' \\ &= \begin{cases} (U - V)(h'(\eta) - h'(0^+)), & \eta \in \hat{C}', \\ (U - V)(h'_C(\eta) - h'(0^+)), & \eta \in \hat{C}, \end{cases}\end{aligned} \tag{3.51}$$

where $\xi = \exp(i2\pi\eta/a)$ as before and $\log(\cdot)$ is the ordinary logarithm defined for positive real numbers.

To proceed further, we require $h'(0^+)$. Since ω^+ is continuous at $\xi = 1$, we conclude from (3.35) that $h'_C(a^-) = h'(0^+)$, provided $V \neq U$. In other words, the continuity of the y-component of velocity precludes any breaks in the slope of the lower boundary of the ice. The local behavior of h and h_C near the contact points $\eta = 0$, $\eta = a$ then requires that $h'_C(a^-) = h'(0^+) = 0$ if the inequality constraints $(3.4)_5$ and $(3.5)_5$ on N and h_C are to be satisfied close to the contact points. To see this, note that the cavity roof is above the sediment surface and we have $h_C(\eta) > h(\eta) = 0$ for $b < \eta < a$, while the cavity roof recontacts the bed at $\eta = a$, so that $h_C(a^-) = 0$ and hence $h'(0^+) = h'_C(a^-) \leq 0$. Meanwhile, $h(\eta) \geq 0$ in contact areas $0 < \eta < b$ (as flux $Vh = q = N \geq 0$ and $V > 0$), and sediment thickness is continuous at the downstream cavity endpoint, so that $h(0) = 0$, which implies $h'_C(a^-) = h'(0^+) \geq 0$. These two inequalities on $h'(0^+)$ can be satisfied simultaneously only if bed and cavity roof slope vanish at the downstream cavity endpoint, $h'(0^+) = h'_C(a^-) = 0$.

An integral equation for h is now straightforward to obtain by integrating (3.51)

once more and using $h(0^+) = 0$:

$$\begin{aligned}(U-V)h(\eta) &= \int_0^\eta (U-V)h'(\eta')\,\mathrm{d}\eta' \\ &= -\frac{1}{2\pi}\int_0^\eta \int_0^b N(\eta')\log\left|\frac{\sin(\pi(\eta'-\eta'')/a)}{\sin(\pi\eta'/a)}\right|\,\mathrm{d}\eta'\,\mathrm{d}\eta'' \\ &= -\frac{1}{2\pi}\int_0^b \left[\int_0^\eta \log\left|\frac{\sin(\pi(\eta'-\eta'')/a)}{\sin(\pi\eta'/a)}\right|\,\mathrm{d}\eta''\right] N(\eta')\,\mathrm{d}\eta' \qquad (3.52)\end{aligned}$$

for $\eta \in (0, b)$. As $h_C(a^-) = 0$ from (3.13), the cavity roof similarly satisfies

$$\begin{aligned}(U-V)h_C(\eta) &= -\int_\eta^a (U-V)h_C(\eta')\,\mathrm{d}\eta' \\ &= \frac{1}{2\pi}\int_0^b \left[\int_\eta^a \log\left|\frac{\sin(\pi(\eta'-\eta'')/a)}{\sin(\pi\eta'/a)}\right|\,\mathrm{d}\eta''\right] N(\eta')\,\mathrm{d}\eta' \qquad (3.53)\end{aligned}$$

for $\eta \in (b, a)$. Solutions of these integral equations automatically satisfy $(3.13)_1$. It remains to ensure that $h_C(b^+) = h(b^-)$. Using (3.52) and (3.53), this can be written in the form

$$\frac{1}{2\pi}\int_0^b \left[\int_0^a \log\left|\frac{\sin(\pi(\eta'-\eta'')/a)}{\sin(\pi\eta'/a)}\right|\,\mathrm{d}\eta''\right] N(\eta')\,\mathrm{d}\eta' = 0. \qquad (3.54)$$

This equation ensures that there is no discontinuity in the ice surface at $\eta = b$, but it generally requires a discontinuity in h (in the sense that (3.54) does not ensure $h(b^-) = 0$). This justifies our statement in section 2 that we cannot generally expect sediment thickness to be continuous across all contact points; this is at least true for traveling wave solutions.

Equation (3.54) allows the integrals above to be simplified somewhat. The kernel on the left-hand side of (3.54) can be rewritten as

$$\begin{aligned}&\int_0^a \log\left|\frac{\sin(\pi(\eta'-\eta'')/a)}{\sin(\pi\eta'/a)}\right|\,\mathrm{d}\eta'' \\ &\quad = \int_0^a \frac{1}{2}\left\{\log\left[4\sin^2\left(\frac{\pi(\eta'-\eta'')}{a}\right)\right] - \log\left[4\sin^2\left(\frac{\pi\eta'}{a}\right)\right]\right\}\,\mathrm{d}\eta''. \qquad (3.55)\end{aligned}$$

But, as shown in the appendix,

$$\int_0^a \log\left[4\sin^2(\pi(\eta'-\eta'')/a)\right]\,\mathrm{d}\eta'' = \int_0^a \log\left[4\sin^2(\pi\eta''/a)\right]\,\mathrm{d}\eta'' = 0, \qquad (3.56)$$

and (3.54) becomes more simply

$$\int_0^b \log\left[4\sin^2(\pi\eta/a)\right] N(\eta)\,\mathrm{d}\eta = 0. \qquad (3.57)$$

Similarly rewriting the integral kernel in (3.52) and (3.53) and using (3.56) and (3.57) yields the integral equations

$$(U-V)h(\eta) = -\frac{1}{4\pi}\int_0^b \left\{\int_0^\eta \log\left[4\sin^2\left(\frac{\pi(\eta'-\eta'')}{a}\right)\right]\,\mathrm{d}\eta''\right\} N(\eta')\,\mathrm{d}\eta' \qquad (3.58)$$

for $\eta \in (0, b)$, and

$$(U-V)h_C(\eta) = -\frac{1}{4\pi}\int_0^b \left\{ \int_0^\eta \log\left[4\sin^2\left(\frac{\pi(\eta'-\eta'')}{a}\right)\right] \mathrm{d}\eta'' \right\} N(\eta')\,\mathrm{d}\eta' \tag{3.59}$$

for $\eta \in (b, a)$.

On writing $N = q = Vh$ and setting $U = 1$ from (3.6) and (3.12), the structure of the problem finally becomes apparent: For a given contact point position b, $h(\eta)$ satisfies the eigenvalue problem

$$\lambda h(\eta) + \int_0^b k(\eta, \eta')h(\eta')\,\mathrm{d}\eta' = 0 \tag{3.60}$$

for $\eta \in (0, b)$, where the kernel k is given by

$$k(\eta, \eta') = \frac{1}{4\pi}\int_0^\eta \log\left(4\sin^2\left[\pi(\eta'-\eta'')/a\right]\right)\,\mathrm{d}\eta'', \tag{3.61}$$

and the real eigenvalue λ is a proxy for pattern velocity V, $\lambda = (1-V)/V$. The contact point b is constrained by (3.54), which reads

$$\int_0^b \log\left[4\sin^2(\pi\eta/a)\right] h(\eta)\,\mathrm{d}\eta = 0. \tag{3.62}$$

Finally, the eigenfunction $h(\eta)$ satisfies the normalization condition (3.47), which becomes

$$\frac{1}{a}\int_0^b h(\eta)\,\mathrm{d}\eta = \lambda + 1. \tag{3.63}$$

Once h, λ, and b have been found, the cavity roof shape $h_C(\eta)$ for $\eta \in (b, a)$ can be calculated from (3.53):

$$\lambda h_C(\eta) = -\int_0^b k(\eta, \eta')h(\eta')\,\mathrm{d}\eta'. \tag{3.64}$$

As mentioned previously, we allow only positive pattern speeds $V > 0$, so $\lambda > -1$, and the mean of h is positive by (3.63). A solution h must further satisfy the stronger pointwise constraint $h(\eta) \geq 0$ for $\eta \in (0, b)$, and similarly $h_C(\eta) > 0$ for $\eta \in (b, a)$. It is by no means obvious that this will be the case: We have so far employed the inequality constraints on h and h_C only locally in order to determine the slopes of h and h_C at the contact points $\eta = 0$, $\eta = a$. Compliance with these constraints must therefore be checked *a posteriori* once a solution has been found. Further, our solution of the Hilbert problems (3.33) and (3.42) requires $N(\eta)$ and $\tau_b(\eta)$ to be Hölder continuous on C'; that is, $h(\eta)$ must be Hölder continuous on $(0, b)$ and (to make sense of the jump conditions (3.13)) continuous up to $\eta = 0$ and $\eta = b$ from the left and right, respectively. Moreover, $h(\eta)$ must satisfy the original integrodifferential equation (3.51), rather than simply the integrated version (3.52). In the appendix, we show that any continuous solution $h \in C([0, b])$ of the eigenvalue problem (3.60)–(3.62) does in fact satisfy this equation and is in $C^1([0, b])$, which takes care of the Hölder continuity of h. Hence it is sufficient to look for continuous $h \in C([0, b])$.

3.4. Numerical method. In order to eliminate the arbitrary wavelength a from the eigenvalue problem, we define

$$X = \eta/a, \qquad B = b/a, \qquad \mu = \lambda/a^2 = (1-V)/(a^2V),$$

$$S(X) = h(\eta), \qquad S_C(X) = h_C(\eta). \tag{3.65}$$

The equations we wish to solve are then

$$\mu S(X) + \frac{1}{4\pi}\int_0^B \left[\int_0^X \log\left[4\sin^2(\pi(X'-X''))\right]\,\mathrm{d}X''\right] S(X')\,\mathrm{d}X' = 0, \tag{3.66}$$

$$\int_0^B \log\left[4\sin^2(\pi X)\right] S(X)\,\mathrm{d}X = 0, \tag{3.67}$$

where the eigenfunction S is to be normalized as

$$\int_0^B S(X)\,\mathrm{d}X = 1 + a^2\mu. \tag{3.68}$$

We are not interested in calculating the entire spectrum of the integral operator in (3.66), but merely seek real eigenvalues $\mu > -1/a^2$. To this end, we can exploit the structure of the integral operator by rewriting (3.66) in the form

$$\begin{aligned}\mu S(X) + \frac{1}{4\pi}\int_0^B \left[\int_0^{X-X'} \log\left[4\sin^2(\pi X'')\right]\,\mathrm{d}X''\right] S(X')\,\mathrm{d}X' \\ = -\frac{1}{4\pi}\int_0^B \left[\int_0^{X'} \log\left[4\sin^2(\pi X'')\right]\,\mathrm{d}X''\right] S(X')\,\mathrm{d}X'.\end{aligned} \tag{3.69}$$

The right-hand side of this equation is simply a constant, while the kernel of the convolution-type integral operator on the left-hand side is antisymmetric and therefore has purely imaginary eigenvalues. It follows that the constant on the right-hand side cannot vanish unless we have the trivial solution $S \equiv 0$, which is, however, precluded by the normalization condition (3.68). If we dispense temporarily with this normalization condition by rescaling S—which we are at liberty to do because (3.66) and (3.67) are homogeneous in S—we can therefore fix the constant on the right-hand side of (3.69) at unity. Denoting this rescaled version of S by $\tilde{S}$, we obtain the pair of equations

$$\mu\tilde{S}(X) + \frac{1}{4\pi}\int_0^B \left[\int_0^{X-X'} \log\left[4\sin^2(\pi X'')\right]\,\mathrm{d}X''\right] \tilde{S}(X')\,\mathrm{d}X' = 1, \tag{3.70}$$

$$-\frac{1}{4\pi}\int_0^B \left[\int_0^{X'} \log\left[4\sin^2(\pi X'')\right]\,\mathrm{d}X''\right] \tilde{S}(X')\,\mathrm{d}X' = 1. \tag{3.71}$$

The advantage of (3.70) is precisely that the kernel of the integral operator on the left-hand side is antisymmetric and hence has purely imaginary eigenvalues. By the Fredholm alternative, (3.70) has a unique solution $\tilde{S}(X;\mu,B) \in C([0,B])$ for every

real nonzero μ and every $B \in (0,1]$. We denote this solution by $\tilde{S}(X;\mu,B)$. In terms of $\tilde{S}(X;\mu,B)$, equations (3.71) and (3.67) can then be written in the form

$$f_1(\mu,B) := \frac{1}{4\pi}\int_0^B \left[\int_0^X \log\left[4\sin^2(\pi X')\right]\,\mathrm{d}X'\right]\tilde{S}(X;\mu,B)\,\mathrm{d}X + 1 = 0, \tag{3.72}$$

$$f_2(\mu,B) := \int_0^B \log\left[4\sin^2(\pi X)\right]\tilde{S}(X;\mu,B)\,\mathrm{d}X = 0. \tag{3.73}$$

The task of finding μ and B can therefore be reduced to solving two nonlinear equations, which must be done numerically. Here we use a backtracking line-search modification of Newton's method [4], where the Jacobian is approximated by finite differences.

In order to evaluate the functions $f_1(\mu,B)$ and $f_2(\mu,B)$, $\tilde{S}(X;\mu,B)$ must be calculated from (3.70). We use a degenerate kernel approximation [2, Chapter 2]: As shown in the appendix, the kernel

$$K(X-X') = \frac{1}{4\pi}\int_0^{X-X'} \log\left[4\sin^2(\pi X'')\right]\,\mathrm{d}X'' \tag{3.74}$$

can be approximated uniformly by the truncated Fourier series

$$K_{n_0}(X-X') = \sum_{n=-n_0,\,n\neq 0}^{n_0} \frac{i\exp(i2n\pi X)\exp(-i2n\pi X')}{8\pi^2|n|n} \tag{3.75}$$

as $n_0 \to \infty$. Replacing $K(X-X')$ by $K_{n_0}(X-X')$, the solution of (3.70) follows the standard method for degenerate kernels.

4. Results and discussion. Regardless of the initial guess for μ and B, only a single solution was found numerically, with $\mu = 2.971\times 10^{-3}$ and $B = 0.2285$. Visual inspection of the surfaces generated by f_1 and f_2 also suggests that this solution is unique. In Figure 4.1, we plot the corresponding shape of $S(X)$ and $S_C(X)$, normalized so that $\int_0^B S(X)\,\mathrm{d}X = 1$ (formally, this is (3.68) with $a = 0$, that is, the short-wave limit). The sediment in the traveling wave is confined to a relatively short wedge upstream of an extended cavity, and the vanishing sediment surface and cavity roof slopes at the contact points $X = 0$, 1 are clearly visible. Moreover, the solution appears to satisfy the constraints $S(X) \geq 0$ for $X \in (0,B)$, $S_C(X) > 0$ for $X \in (B,1)$. Note that a solution $S(X)$ for a given wavelength $a \neq 0$ can be obtained from that plotted in Figure 4.1 simply by multiplying it by $1 + a^2\mu$. This ensures that the normalization condition (3.68) is satisfied. Since the amplitude of S varies with wavelength as $1+a^2\mu$, we see that long waves are also taller than short ones. Furthermore, the pattern speed V can be calculated as $V = 1/(1+a^2\mu)$, which states that pattern speed is inversely proportional to amplitude and hence that shorter waves travel faster than longer ones. Moreover, since $\mu > 0$, the pattern speed V is always less than the ice velocity U. If we take a to be given as the fastest growing wavelength in the original instability model in section 2, then $a = 2\pi[2/\sqrt{3}]^{1/2} = 6.752$ and $V = 0.881$. These traveling waves are advected downstream at 88% of the velocity of ice at the bed, and their amplitude is 1.135 times that shown in Figure 4.1.

The existence of a traveling wave solution suggests that cavity formation may be sufficient to lead to bounded growth in the instability mechanism proposed by Hindmarsh [11] and Fowler [8]. However, it also poses some interesting open questions

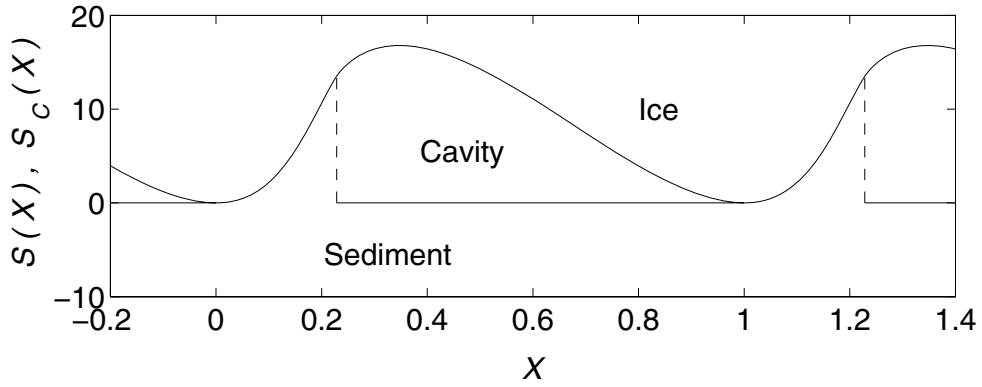

FIG. 4.1. *Solution $S(X)$ for sediment surface elevation and $S_C(X)$ for cavity roof elevation, normalized so that $\int_0^B S(X)\,\mathrm{d}X = 1$ and extended periodically. The sediment shock at $X = B$ is shown as a dashed vertical line.*

regarding the dynamical problem of section 2: First, are the traveling waves described here stable to small perturbation, and if so, does their stability depend on their wavelength? Second, how do waves of different wavelengths interact? Do shorter waves merge with larger ones, and does wavelength coarsening occur? The first of these questions may be amenable to a complex variable approach of the type used above, using an appropriate linearization. The second is much harder and requires an understanding of the fully nonlinear time-dependent problem.

Physically, our results also pose some additional questions. Following [11, 8], our model assumes that porewater pressure in the sediment, and hence mean effective pressure, are fixed by a pre-existing subglacial drainage system, most likely taking the form of channels at the ice-bed interface [15]. However, once cavities have formed, it is likely that they will serve as both storage volume and conduits for water flowing beneath the glacier, and that drainage through these cavities will be instrumental in controlling water pressures at the bed. The simplest way to understand how this type of drainage might work is by considering cavities as a kind of macroscopic pore space, and to consider drainage through cavities at the bed as being a two-dimensional analogue of drainage in ordinary porous media, giving rise to a Biot-type problem [7, 10] for water pressure on an outer length scale associated with the length of the glacier as a whole (which is assumed to be large compared with the instability length scale considered in the model studied in this paper). The problem with applying this approach here is that the size of cavities increases with mean effective pressure (scaled to unity in the dimensionless model), as can be shown from the scalings used in [19]. Specifically, the dimensional scale for h is

$$[h] = \frac{[N]}{(n-2)(1-\phi)(\rho_s - \rho_w)g},$$

where $[N]$ is mean effective pressure at the bed ("mean" being an average taken over the cavity length scale), n is an exponent in the assumed power-law rheology for sediment (which gives rise to the constitutive relations for shear stress τ_b and flux q in (2.6) for $n \gg 1$; see [19]), ϕ is the porosity of the sediment, ρ_s and ρ_w are the densities of sediment grains and of water, and g is acceleration due to gravity. Hence $[h]$ increases linearly with effective pressure, and it follows that cavity size *decreases*

with water pressure. This in turn means that the advocated Biot-type drainage model takes the form of a backward diffusion problem and is therefore ill-posed.

It is unclear to what extent this result is due to the particular rheological model employed for subglacial sediment, and an obvious avenue for further research is to consider alternative prescriptions for τ_b and q from those introduced in (2.6). The eigenvalue problem (3.58) combined with constraints of the form (3.47) and (3.54) generalizes relatively easily to other forms of τ_b and q, though the resulting nonlinear eigenvalue problem is considerably more complicated [16], and we leave a solution as an open problem.

Appendix. Smoothness of solutions. It can be shown in the usual way from the Arzelà–Ascoli theorem that the integral operator in (3.70) is compact on $C([0,B])$, and the antisymmetry of the kernel further ensures that all its eigenvalues are purely imaginary. By the Fredholm alternative [3, Chapter 7.5], the integral equation (3.70) therefore has a unique solution in $C([0,B])$ for every real μ. In what follows, we will show that this solution is in fact in $C^1([0,B])$ and satisfies the integrodifferential equation (3.51). In the process, we will also prove (3.56) and show that the degenerate kernel approximation (3.75) converges uniformly to K in the limit $n_0 \to \infty$.

At issue is thus whether a solution of (3.70) satisfies (3.51), which in view of (3.54), (3.6), (3.12), and the rescaling in (3.65) may be rewritten in the form

$$-\frac{1}{4\pi}\int_0^b \log\left(4\sin^2[\pi(X-X')]\right)\tilde{S}(X)\,\mathrm{d}X' = \mu\tilde{S}'(X) \tag{A.1}$$

for $X \in (0,B)$. If $\tilde{S} \in C([0,B])$ satisfies (A.1), it follows immediately from the properties of convolution integrals that $\tilde{S}' \in C([0,B])$, and $\tilde{S} \in C^1([0,B])$, as required. Equation (A.1) can be obtained by differentiating (3.70) (noting that the right-hand side is simply a constant) and by exchanging the order of differentiation and integration on the integral term. In order to prove that integration and differentiation do commute—which is not obvious because the integrand in (A.1) has a singularity—we approximate the integrand by a sequence of bounded integrands.

A.1. Degenerate kernel approximation. The power series

$$\sum_{n=1}^{\infty}\frac{\zeta^{n-1}}{n} = -\frac{\log(1-\zeta)}{\zeta}$$

has radius of convergence one, and therefore converges everywhere inside the unit circle in the complex ζ-plane. The branch of the logarithm must be continuous on the open unit disk with $\log(1)=0$. Note that the singularity at the origin is removable: We can assign $-\frac{1}{\zeta}\log(1-\zeta)$ its limiting value of 1. The series also converges pointwise on the unit circle except at $\zeta = 1$ [1, p. 409]. For ξ on the unit circle and $r \in (0,1)$, we have

$$\left|\sum_{n=1}^{n_0}\frac{r^{n-1}\xi^n}{n}\right| \le \sum_{n=1}^{n_0}\left|\frac{r^{n-1}\xi^n}{n}\right| = \sum_{n=1}^{n_0}\frac{r^{n-1}}{n} < \frac{\log(1-r)}{r} \tag{A.2}$$

for any finite n_0. Since $\frac{1}{r}\log(1-r)$ is integrable over $r \in (0,1)$, so is

$$\sum_{n=1}^{\infty}\frac{r^{n-1}\xi^n}{n} = -\frac{\log(1-r\xi)}{r\xi}\xi,$$

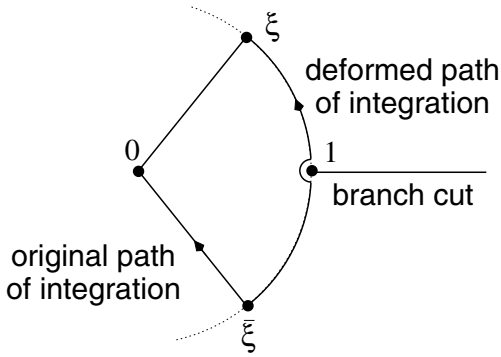

FIG. A.1. *Integration paths in the degenerate kernel approximation of* $K(x)$.

and the order of summation and integration may be interchanged by the dominated convergence theorem, i.e.,

$$\int_0^1 -\frac{\log(1-r\xi)}{r\xi}\xi\,\mathrm{d}r = \sum_{n=1}^{\infty}\int_0^1 \frac{(r\xi)^{n-1}}{n}\xi\,\mathrm{d}r = \sum_{n=1}^{\infty}\frac{\xi^n}{n^2}. \tag{A.3}$$

Similarly,

$$\int_0^1 -\frac{\log(1-r\bar{\xi})}{r\bar{\xi}}\bar{\xi}\,\mathrm{d}r = \sum_{n=1}^{\infty}\frac{\bar{\xi}^n}{n^2}. \tag{A.4}$$

Subtracting the last two expressions and recognizing that $\bar{\xi} = 1/\xi$ yields

$$\sum_{n=-\infty,\, n\neq 0}^{\infty}\frac{\xi^n}{n|n|} = \int_0^1 -\frac{\log(1-r\xi)}{r\xi}\xi\,\mathrm{d}r - \int_0^1 -\frac{\log(1-r\bar{\xi})}{r\bar{\xi}}\bar{\xi}\,\mathrm{d}r. \tag{A.5}$$

However, the right-hand side is just the integral $\int -\frac{1}{\zeta}\log(1-\zeta)\,\mathrm{d}\zeta$ taken along the radial path from $\bar{\xi}$ to ξ via the origin (see Figure A.1). Since the integrand $-\frac{1}{\zeta}\log(1-\zeta)$ can be made holomorphic in the complex plane cut along the interval $[1,\infty)$ on the real line, the curve along which the integral is taken can be deformed to lie on the unit circle, with a small indentation at the branch point $\zeta = 1$ (Figure A.1). The indentation does not contribute to the integral along the deformed curve in the limit where the radius of the indentation tends to zero. Setting $\xi = \exp(i2\pi X)$, the integral may thus be expressed as

$$\begin{aligned}\sum_{n=-\infty,\, n\neq 0}^{\infty}\frac{\xi^n}{n|n|} &= -i2\pi\int_{-X}^{X}\log\left[1-\exp(i2\pi X')\right]\,\mathrm{d}X' \\ &= -i2\pi\int_{0}^{X}\log\left[1-\exp(i2\pi X')\right] + \log\left[1-\exp(-i2\pi X')\right]\,\mathrm{d}X' \\ &= -i2\pi\int_{0}^{X}\log\left[4\sin^2(\pi X')\right]\,\mathrm{d}X'. \end{aligned} \tag{A.6}$$

Consequently, the kernel K defined by (3.74) may be written as

$$K(X) = \frac{1}{4\pi}\int_0^X \log\left[4\sin^2(\pi X')\right]\,\mathrm{d}X' = \sum_{n=-\infty,\, n\neq 0}^{\infty} \frac{i\xi^n}{8\pi^2 n|n|}. \tag{A.7}$$

The argument above has shown that the series on the right converges pointwise to the integral in the middle. By the Weierstrass M-test, it also converges uniformly; that is, $K_{n_0}(X)$ defined in (3.75) converges to $K(X)$ in the $C([0,B])$ norm as $n_0 \to \infty$.

Lastly, it follows immediately that $K(1) = 0$, and (3.56) holds.

A.2. Differentiation under the integral sign. We can use the series representation (A.7) of the kernel K to show that (A.1) holds. Specifically, let

$$\mu\tilde{S}_{n_0}(X) = -\int_0^B K_{n_0}(X - X')\tilde{S}(X')\,\mathrm{d}X' + 1, \tag{A.8}$$

where K_{n_0} is defined in (3.75). It is easy to see that $\tilde{S}_{n_0}$ converges to $\tilde{S}$ in the $C([0,B])$ norm. Since K'_{n_0} is continuous and hence bounded, we can further differentiate directly,

$$\mu\tilde{S}'_{n_0}(X) = -\int_0^B K'_{n_0}(X - X')\tilde{S}(X')\,\mathrm{d}X', \tag{A.9}$$

and $\tilde{S}_{n_0} \in C^1([0,B])$. But $K'_{n_0}(X) = -\sum_{n=-n_0,n\neq 0}^{n_0} \exp(i2\pi X)/(4\pi n)$ converges to $K'(X)$ almost everywhere in $[0,1]$ by the results of section A.1. Moreover, because $\sum_{n=1}^{\infty} 1/|n|^2 < \infty$, $K'_{n_0}(X)$ also converges as a Fourier series to $K'(X)$ in the $L^2([0,1])$-norm, and hence in the $L^1([0,1])$-norm. Hence, for $B \in [0,1]$,

$$\begin{aligned}\sup_{x\in[0,B]} &\left|\int_0^B K'_{n_0}(X - X')\tilde{S}(X')\,\mathrm{d}X' - \int_0^B K'(X - X')\tilde{S}(X')\,\mathrm{d}X'\right| \\ &\leq \sup_{X\in[0,B]} |\tilde{S}(X)| \int_0^1 \left|K'_{n_0}(X') - K'(X')\right|\,\mathrm{d}X' \to 0\end{aligned} \tag{A.10}$$

as $n_0 \to \infty$. By the completeness of $C^1([0,B])$, we therefore have

$$\mu\tilde{S}'(X) = \mu\frac{\mathrm{d}}{\mathrm{d}X}\lim_{n_0\to\infty}\tilde{S}_{n_0}(X) = -\int_0^B K'(X - X')\tilde{S}(X')\,\mathrm{d}X', \tag{A.11}$$

which is (A.1).

REFERENCES

[1] T. M. Apostol, *Calculus*, 2nd ed., Blaisdell Publishing, Waltham, MA, 1969.

[2] K. E. Atkinson, *The Numerical Solution of Integral Equations of the Second Kind*, Cambridge Monogr. Appl. Comput. Math. 88, Cambridge University Press, Cambridge, UK, 1997.

[3] E. W. Cheney, *Analysis for Applied Mathematics*, Grad. Texts in Math. 208, Springer-Verlag, New York, 2001.

[4] J. E. Dennis, Jr., and R. B. Schnabel, *Numerical Methods for Unconstrained Optimization and Nonlinear Equations*, Classics in Appl. Math. 16, SIAM, Philadelphia, 1996.

[5] A. H. England, *Complex Variable Methods in Elasticity*, J. Wiley & Sons, London, 1971.

[6] A. C. Fowler, *A sliding law for glaciers of constant viscosity in the presence of subglacial cavitation*, Proc. R. Soc. Lond. Ser. A Math. Phys. Eng. Sci., 407 (1986), pp. 147–170.

[7] A. C. Fowler, *Sliding with cavity formation*, J. Glaciol., 33 (1987), pp. 255–267.
[8] A. C. Fowler, *An instability mechanism for drumlin formation*, in Deformation of Glacial Materials, A. Maltman, M. J. Hambrey, and B. Hubbard, eds., Spec. Pub. Geol. Soc. 176, The Geological Society, London, 2000, pp. 307–319.
[9] A. C. Fowler, *Evolution equations for dunes and drumlins*, Rev. P. Acad. Cien. Ser. A Mat., 96 (2002), pp. 377–387.
[10] A. C. Fowler and C. G. Noon, *Mathematical models of compaction, consolidation and regional groundwater flow*, Geophys. J. Int., 136 (1999), pp. 251–260.
[11] R. C. A. Hindmarsh, *The stability of a viscous till sheet coupled with ice flow, considered at wavelengths less than the ice thickness*, J. Glaciol., 44 (1998), pp. 285–292.
[12] B. Kamb, *Basal zone of the West Antarctic ice streams and its role in lubrication of their rapid motion*, in The West Antarctic Ice Sheet: Behaviour and Environment, R. B. Alley and R. A. Binschadler, eds., American Geophysical Union, Washington, DC, 2001, pp. 157–199.
[13] N. Kikuchi and J. T. Oden, *Contact Problems in Elasticity: A Study of Variational Inequalities and Finite Element Methods*, SIAM Stud. Appl. Math. 8, SIAM, Philadelphia, 1988.
[14] N. I. Muskhelishvili, *Singular Integral Equations*, Dover Publications, New York, 1992.
[15] F. S. L. Ng, *Mathematical Modelling of Subglacial Drainage and Erosion*, D. Phil. Thesis, Mathematical Institute, Oxford University, 1998; available online at http://www.maths.ox.ac.uk/research/theses/.
[16] C. Schoof, *Mathematical Models of Glacier Sliding and Drumlin Formation*, D. Phil. Thesis, Mathematical Institute, Oxford University, 2002; available online at http://www.maths.ox.ac.uk/research/theses/.
[17] C. Schoof, *The effect of cavitation on glacier sliding*, Proc. R. Soc. Lond. Ser. A Math. Phys. Eng. Sci., 461 (2005), pp. 609–627.
[18] C. Schoof, *A variational approach to ice-stream flow*, J. Fluid Mech., 556 (2006), pp. 227–251.
[19] C. Schoof, *Pressure-dependent viscosity and interfacial instability in coupled ice-sediment flow*, J. Fluid Mech., 570 (2007), pp. 227–252.
[20] S. Tulaczyk, *Ice sliding over weak, fine-grained till: Dependence of ice-till interactions on till granulometry*, Spec. Paper Geol. Soc. Am., 337 (1999), pp. 159–177.